

# Mechanosynthesis of $\text{Hf}_{1-x}\text{Zr}_x\text{B}_2$ Solid Solution and $\text{Hf}_{1-x}\text{Zr}_x\text{B}_2/\text{SiC}$ Composite Powders

Miguel A. Avilés, Jose M. Córdoba, María J. Sayagués, María D. Alcalá, and Francisco J. Gotor<sup>†</sup>

Instituto de Ciencia de Materiales de Sevilla (CSIC-US), 41092 Sevilla, Spain

The synthesis of solid solutions in the  $\text{HfB}_2\text{--ZrB}_2$  system was conducted by mechanically induced self-sustaining reaction (MSR) processes under an inert atmosphere from elemental mixtures of Hf, Zr, and B. The stoichiometry of the  $\text{Hf}_{1-x}\text{Zr}_x\text{B}_2$  solid solution phase was controlled by adjusting the Hf/Zr/B atomic ratio in the starting mixture. Composite materials with SiC were achieved by adding the required amount of SiC to the Hf/Zr/B reactant mixture. The presence of up to 20 vol% of SiC did not inhibit the MSR process. Longer milling times were required to ignite the mixture. Small amounts of the refractory phases ZrC or HfC were observed in the composite powders. The chemical composition, structure, and microstructure of products were studied by X-ray diffraction, scanning and transmission electron microscopy, electron diffraction, and energy-dispersive X-ray spectroscopy. This complete characterization confirmed the formation of  $P6/mmm$  hexagonal diboride phases with a submicrometric microstructure. The determination of the chemical composition and lattice parameters ascertained the formation of solid solutions with good chemical homogeneity in the  $\text{HfB}_2\text{--ZrB}_2$  system.

## I. Introduction

**H**AFNIUM DIBORIDE ( $\text{HfB}_2$ ) and zirconium diboride ( $\text{ZrB}_2$ ) have an excellent combination of physical and chemical properties—high melting temperature, high hardness, low electrical resistivity, chemical inertness, and high thermal stability—that make them extremely interesting for high-temperature applications.<sup>1</sup> A new emerging family of materials able to withstand ultra-high temperatures is under development based on these refractory compounds.<sup>2</sup> These materials, called ultra-high-temperature ceramics (UHTCs), can potentially be used at temperatures above 1800°C because of their outstanding thermal and chemical stability, strength at high temperatures, and oxidation resistance.<sup>3–5</sup> UHTCs are currently composed of  $\text{HfB}_2$  and  $\text{ZrB}_2$  as binary compounds, and as composites with silicon carbide (SiC). The inclusion of SiC improves the oxidation resistance, densification, and thermal shock of  $\text{HfB}_2\text{--SiC}$  and  $\text{ZrB}_2\text{--SiC}$  composites.<sup>6,7</sup> In these composites, a complex oxide scale constituted of a refractory oxide skeleton and amorphous glass components form after high-temperature oxidation, reducing oxygen permeability, and providing improved high-temperature resistance.<sup>8</sup>

$\text{HfB}_2$  and  $\text{ZrB}_2$  possess the same  $\text{AlB}_2$ -type crystal structure,<sup>9</sup> which is depicted by a graphite-like honeycomb geometry of layers of boron separated by a hexagonal layer (h.c.p.) of transition metal. The boron nets have very strong covalent bonds that hinder an increase in the  $a_0$  direction, although no such

hindrance occurs in the  $c_0$  direction, giving borides the ability to accommodate a wide variety of metals. As Hf and Zr have similar atomic radii, a continuous solid solution is possible in the  $\text{HfB}_2/\text{ZrB}_2$  system. The properties of these solid solutions, such as thermal expansion coefficient or hardness, could be tailored by controlling their stoichiometry.<sup>8</sup> Consequently, the use of these solid solution-based compositions would permit designers to modulate the material properties depending on the requirements for different technological applications. The formation of solid solutions in the  $\text{HfB}_2/\text{ZrB}_2$  system has been revealed after the high-temperature processing of UHTCs, including both diborides.<sup>10</sup> However, it is expected that the use of pre-made solid solutions, instead of unalloyed mixtures as the raw material, would permit a higher level of quality and reliability to be achieved in the final properties. In this case, it would be necessary to find an affordable and reproducible manufacturing process for these solid solutions.

The reaction synthesis of  $\text{HfB}_2$  and  $\text{ZrB}_2$  from the mixture of their elements is an extremely exothermic process ( $\Delta H_{298}^\circ = -79.06$  and  $-77.84$  kcal/mol for  $\text{HfB}_2$  and  $\text{ZrB}_2$ , respectively),<sup>11</sup> and it has already been shown that they can be obtained by self-propagating high-temperature synthesis (SHS).<sup>12,13</sup> Highly exothermic chemical reactions can also be induced by high-energy ball milling<sup>14,15</sup> leading to a self-sustaining reaction within the milling bowl after a critical milling time, called the ignition time.<sup>16</sup> This kind of process, denoted as a mechanically induced self-sustaining reaction (MSR),<sup>17</sup> is similar to thermally ignited SHS. Initially, in an MSR process, milling results in activation, similar to any other mechanical alloying process. During this time, size reduction and mixing occur, and chemically active sites and defects are created, but little product is formed. At the ignition time, the reaction rate increases abruptly leading to a self-sustaining process where most of the reactants are consumed and transformed into products instantaneously. This fact reduces the milling time needed to obtain a high yield of product and, therefore, the contamination resulting from the grinding media, as generally observed in conventional milling processes. In contrast to SHS, MSR allows the mixing of reactants, product yield, and its subsequent homogenization in one single step.

Some authors have reported that milling processes associated with the formation of  $\text{HfB}_2$  and  $\text{ZrB}_2$  from their elements can occur through a self-sustaining reaction depending on the milling intensity.<sup>18,19</sup> MSR is a promising method and a practical means for the production of  $\text{HfB}_2$  and  $\text{ZrB}_2$  because it is fast, simple, direct, and uses self-generated heat to achieve full conversion. These characteristics contrast with the high energetic requirements (temperatures of  $\sim 2000^\circ\text{C}$  are generally used) and difficulties of the common production methods based on reduction processes like borothermal reduction,<sup>20</sup> boro/carbothermal reaction<sup>21</sup> or the reaction between a metal oxide and boron oxide via carbothermal reduction.<sup>22</sup>

Some works have already reported the formation of solid solutions in transition metal diboride systems and, in general, they are produced by annealing the mixtures of the two end members at high temperatures.<sup>23–25</sup> Only a few papers deal with the synthesis of solid solutions using elemental reactants and combustion-like processes.<sup>26</sup> In this work, we present results

Y. Zhou—contributing editor

Manuscript No. 26600. Received August 5, 2009; approved October 7, 2009. This work was supported by the Spanish Government under Grant No. MAT2006-04911.

<sup>†</sup>Author to whom correspondence should be addressed. e-mail: fgotor@cica.es

concerning the synthesis of  $HfB_2$ ,  $ZrB_2$ , and their solid solution  $Hf_{1-x}Zr_xB_2$ . Synthesis is conducted with different Hf/Zr atomic ratios by high-energy ball milling through an MSR process from powder mixtures of elemental zirconium and hafnium with amorphous boron. We have also focused on integrating MSR within the methodology for synthesizing composite materials in the  $HfB_2$ - $ZrB_2$ -SiC system, which are the main components in UHTCs.

## II. Experimental Procedure

Hafnium powder (99.6% in purity, <325 mesh, Alfa Aesar, Ward Hill, MA), zirconium powder (<325 mesh, Alfa Aesar), boron powder (95–97% in purity, amorphous powder, Fluka, St. Louis, MO), and SiC powder (<400 mesh, Fluka) were used in this work. The different powder mixtures were ball milled under six bars of high-purity helium gas ( $H_2O < 3$  ppm,  $O_2 < 2$  ppm, and  $CnHm < 0.5$  ppm, Air Liquide, Paris, France) using a modified planetary ball mill (model Micro Mill Pulverisette 7, Fritsch, Idar-Oberstein, Germany). Five grams of powder, together with seven tempered steel balls, were placed in a tempered steel vial (67 Rc) for each milling experiment. The volume of the vial was 45 mL. The diameter and weight of the balls were 15 mm and 12.39 g, respectively. The powder-to-ball mass ratio (PBR) was 1/17.35. The vial was purged with helium gas several times, and the desired pressure was selected before milling. The vial was connected to the gas cylinder during the milling experiments by a rotating union and a flexible polyamide tube. A spinning rate of 600 rpm for both the rotation of the supporting disk and the superimposed rotation in the direction opposite to the vial was always used.

The helium pressure was continuously monitored during the milling process by an SMC Solenoid Valve (model EVT307-5DO-01F-Q, SMC Co.). When the MSR occurred, the increasing temperature due to the exothermic reaction produced an instantaneous increase in the total pressure. The ignition time for the different mixtures, e.g., the milling time required to produce the combustion process, was obtained from the time–pressure record. After ignition, milling was prolonged for 30 min in order to obtain a homogeneous product.

X-ray powder diffraction (XRD) patterns of products were acquired with a Siemens instrument (model D501, Munich, Germany) equipped with a scintillation counter using  $CuK\alpha$  radiation and a graphite monochromator. Data were collected in the range of  $20^\circ$ – $130^\circ$  ( $2\theta$ ) in step-scan mode with a step of  $0.02^\circ$  and a counting time of 10 s/step. Lanthanum hexaboride powder (Standard Reference Material 660a, NIST) was used to correct XRD shift peaks and instrumental line broadening. Lattice parameters were calculated from the entire set of peaks of the XRD diagram ( $20^\circ$ – $130^\circ$ ; 21 peaks) using the Fullprof computer program, assuming a hexagonal symmetry.<sup>27</sup> The separation of grain size and strain contributions to the broadening of XRD peaks was performed by applying the following equation<sup>28</sup>:

$$\frac{\beta^2}{\tan^2 \theta} = \frac{K\lambda}{D} \left( \frac{\beta}{\tan \theta \sin \theta} \right) + 16e^2 \quad (1)$$

which assumes a Gaussian function for the strain broadening and a Cauchy function for the effects of crystallite size and size distributions, and where  $\beta$  is the integral breadth,  $\theta$ , the position of peak maximum,  $K$  is a factor taken as 0.9,  $\lambda$  is the  $CuK\alpha_1$  radiation,  $D$  is the average crystallite size, and  $e$  is the maximum strain. A linear plot of  $\beta^2/\tan^2 \theta$  against  $\beta/\tan \theta \sin \theta$  allows the determination of the crystallite size,  $D$ , from the slope, and the maximum strain,  $e$ , from the ordinate intercept.

Scanning electron microscopy (SEM) and energy-dispersive X-ray (EDX) analysis were performed in a Hitachi FEG S-4800 microscope (Tokyo, Japan). Transmission electron microscopy (TEM), electron diffraction (ED), and EDX experiments were performed using a 200 kV Philips CM-200 microscope (Amsterdam, the Netherlands) with a supertwin objective lens, a

$LaB_6$  filament, and a  $\pm 45^\circ$  tilt side-entry specimen holder (point resolution = 0.24 nm). The instrument was equipped with an EDS detector (EDAX Inc., Mahwah, NJ) for chemical analysis. Powder samples were dispersed in ethanol and deposited onto a holey carbon grid.

## III. Results and Discussion

Table I shows the different elemental mixtures submitted to high-energy ball milling in order to obtain the binary diborides,  $HfB_2$  and  $ZrB_2$ , and their solid solution  $Hf_{1-x}Zr_xB_2$  with three Hf/Zr atomic ratios (3/1, 1/1, and 1/3). Composite materials with 10 and 20 vol% of SiC were obtained by adding the required amount of SiC to the reactant Hf/Zr/B mixture. In all cases, an MSR was detected during milling, and the XRD patterns of the products always showed the formation of hexagonal diboride phases (Fig. 1).

The self-heating capacity of mixtures submitted to milling determines the appearance of the MSR process. This capacity is connected with the adiabatic temperature ( $T_{ad}$ ), which is defined as the maximum temperature reached by the products due to the reaction heat if it occurs in an isolated system. This temperature is a rough indicator of whether a reaction is possible by self-propagation or not. It has been empirically proposed for SHS processes that they can take place if this temperature is higher than 1800 K.<sup>29</sup> The same rule could also be applied for MSR processes. Nevertheless, during milling, the reactant mixture is in contact with the grinding media, and larger heat loss to the environment than in the SHS process occurs. Consequently, an MSR process will only occur if the adiabatic temperature is well above the limit of 1800 K.<sup>16</sup> This empirical limit can be calculated from the thermodynamic functions of heat capacities and enthalpies of formation and transformation of products. If the following condition is fulfilled:

$$\Delta H_{298}^\circ < \int_{298}^{T_m} C_{ps} dT \quad (2)$$

the adiabatic temperature is lower than the melting temperature of the product ( $T_m$ ) and it can be obtained from the following expression:

$$\Delta H_{298}^\circ = \int_{298}^{T_{ad}} C_{ps} dT \quad (3)$$

where  $\Delta H_{298}^\circ$  is the enthalpy of formation of the product at 298 K, and  $C_{ps}$  is the heat capacity in the solid state. As data of enthalpies of formation and heat capacities are not available in the literature for the chemical systems studied in this work, the averaged values from the formation enthalpies of the binary compounds and the heat capacity of the elements have been

**Table I. Different Mixtures Submitted to High-Energy Ball Milling**

Sample	Starting powder mixtures (elemental atomic ratio)	$T_{ad}$ (K)	$t_{ig}$ (min)
1	Hf/B (1/2)	3336	24
2	Hf/Zr/B (3/1/8)	3271	27
3	Hf/Zr/B (1/1/4)	3203	24
4	Hf/Zr/B (1/3/8)	3196	31
5	Zr/B (1/2)	3163	23
6	Hf/B (1/2)+10 vol% SiC	3130	30
7	Hf/Zr/B (1/1/4)+10 vol% SiC	3062	35
8	Zr/B (1/2)+10 vol% SiC	3030	58
9	Hf/B (1/2)+20 vol% SiC	2992	49
10	Hf/Zr/B (1/1/4)+20 vol% SiC	2901	55
11	Zr/B (1/2)+20 vol% SiC	2867	64

Adiabatic temperatures ( $T_{ad}$ ), and ignition times ( $t_{ig}$ ) observed during the MSR process are included. MSR, mechanically induced self-sustaining reaction.

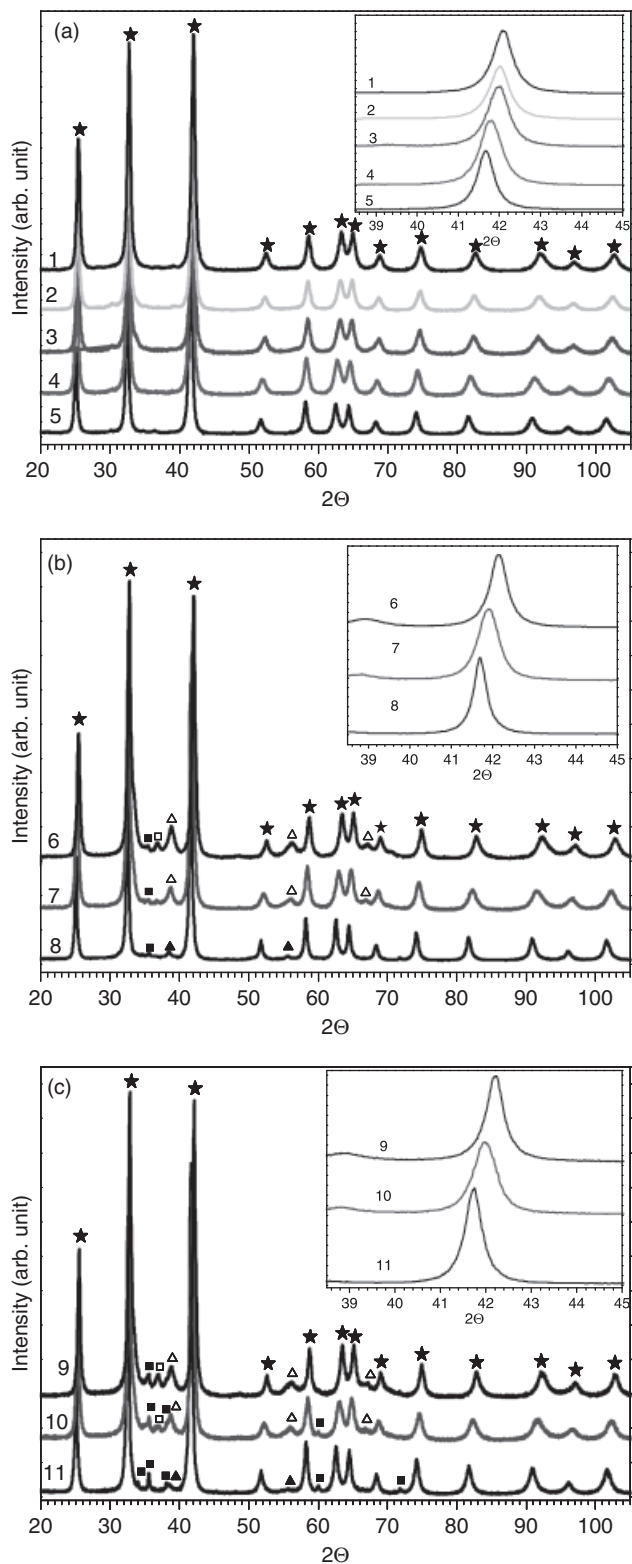


**Fig. 1.** X-ray powder diffraction patterns of the products after the mechanically induced self-sustaining reaction process from the starting mixtures in Table I: (a) without SiC (samples 1–5), (b) with 10 vol% of SiC (samples 6–8), and (c) with 20 vol% of SiC (samples 9–11). (★)  $P6/mmm$  hexagonal diboride phase; (■), SiC; (▲), ZrC; (△), HfC; (□), Hf.

used. Table II presents the thermodynamic data used in the calculation,<sup>11,30</sup> and the adiabatic temperatures of different mixtures are presented in Table I. In all cases, the adiabatic temperature was much higher than the empirical limit of 1800 K. Table I shows that the addition up to 20 vol% of SiC reduced the value of the adiabatic temperature by about 10% and the

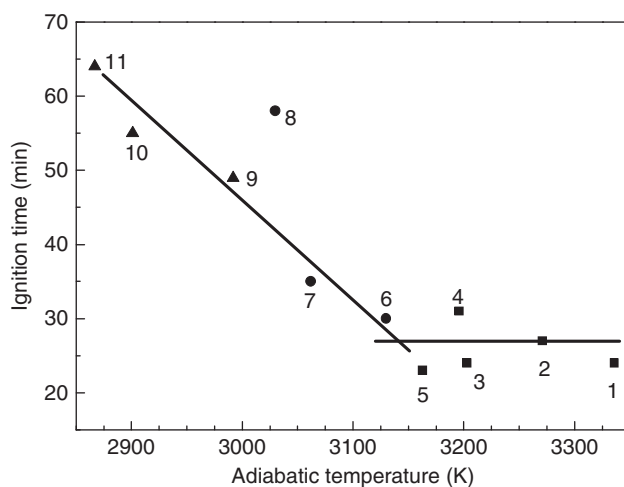


**Fig. 2.** Ignition time versus adiabatic temperature for mixtures in Table I (numbers correspond to the label of samples in this table). (■), Hf/Zr/B mixtures; (●), mixtures with 10 vol% of SiC; (▲), mixtures with 20 vol% of SiC.

MSR process was not inhibited. Although the peritectic decomposition of SiC ( $\sim 2800$ – $3100$  K depending on the authors<sup>31</sup>) is of the same order as the adiabatic temperatures obtained for the mixtures containing SiC, this decomposition has not been taken into consideration in the calculation of the adiabatic temperature because the exact temperature of this peritectic decomposition is not well established in the literature. In any case, the low content of SiC in the mixtures renders the influence of this decomposition on the value of the adiabatic temperature insignificant.

The values of the ignition time ( $t_{ig}$ ) for the different mixtures were measured from the time–pressure records, and are also included in Table I. A straightforward relation between ignition time and adiabatic temperature was not found. Although a minimum adiabatic temperature is a necessary condition to produce the MSR reaction, its value is not the only parameter that influences the ignition time. Nevertheless, the plot of  $t_{ig}$  versus the adiabatic temperature evidenced, in fact, two different regions (Fig. 2). For adiabatic temperatures above 3100 K, a nearly constant ignition time was observed, indicating that Zr/B and Hf/B systems behave in a similar way regarding the MSR process. However, below this temperature, for mixtures containing SiC, the general trend of longer ignition times for lower adiabatic temperatures was noticed;  $t_{ig}$  increased as the amount of SiC increased. As this phase does not take part in the

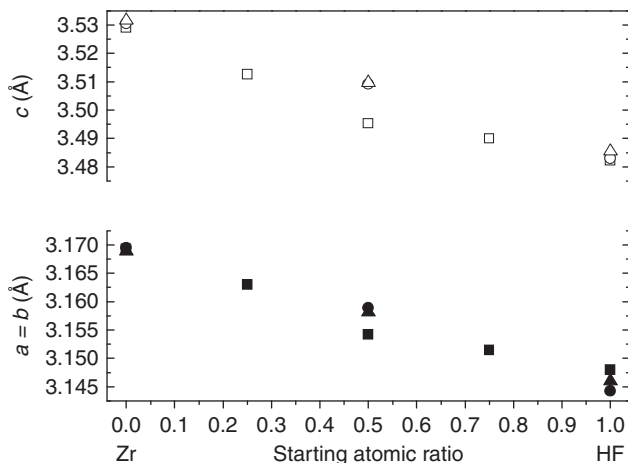


**Fig. 3.** Lattice parameters,  $a$  and  $c$ , of the  $P6/mmm$  hexagonal diboride phase obtained after the mechanically induced self-sustaining reaction process from the starting mixtures in Table I. (■), □, mixtures without SiC; (●), ○, mixtures with 10 vol% of SiC; (▲), △, mixtures with 20 vol% of SiC.

**Table II.** Enthalpies of Formation and Heat Capacities Used in the Calculation of the Adiabatic Temperatures from Eq. (3)<sup>9,28</sup>

Compound or element	Melting point (K)	$\Delta H_{f298}^\circ$ (kcal/mol)	$C_p = a + (b \times 10^{-3})T + (c \times 10^{-6})T^2 + (d \times 10^5)T^{-2}$ (cal (g·mol) <sup>-1</sup> )			
			<i>a</i>	<i>b</i>	<i>c</i>	<i>d</i>
HfB <sub>2</sub>	3370	-79.06	6.00	0.52	—	1.812
ZrB <sub>2</sub>	3273	-77.84	6.83	1.12	—	-0.870
Hf			1.54	4.40	—	—
Zr			5.70	1.02	—	-1.060
B			4.10	1.02	—	-2.100
Si						
C						

self-sustaining reaction, it behaves inertly, removing reaction heat from the powder mixture and delaying the ignition.

As mentioned above, the XRD patterns of different products obtained after the MSR process (Fig. 1) confirmed the formation of *P6/mmm* hexagonal diboride phases. In samples 1 to 5, no other peak indicative of unreacted Hf or Zr or undesired phases was detected, suggesting complete phase conversion of the reactants into products. Obviously, in samples 6–11, the XRD peaks corresponding to SiC were observed, but those corresponding to HfC or ZrC were identified as well. In samples 6, 9, and 10, trivial amounts of unreacted Hf were distinguished. The presence of the carbide phases indicates that high temperatures were locally reached inside the milling vial as a direct consequence of the self-sustaining reaction, inducing the decomposition of SiC and the subsequent formation of carbides. As previously pointed out, the peritectic decomposition temperature of SiC could have been reached during the MSR process. Quantitative analyses performed from XRD measurements using the Fullprof computer program showed that about 30% and 15% of SiC in composite mixtures containing 10 and 20 vol%, respectively, were decomposed during the MSR process.

The position of XRD peaks in samples 1, 6, and 9 matches with the JCPDS data file 38-1398 (HfB<sub>2</sub>), and in the case of samples 5, 8, and 11 with the JCPDS data file 34-0423 (ZrB<sub>2</sub>). However, in samples 2, 3, 4, 7, and 10, where ternary mixtures of Hf, Zr, and B were milled, the XRD peaks of the diboride phase fall between those corresponding to the binary HfB<sub>2</sub> and ZrB<sub>2</sub>, as it is clearly revealed in the onsets of Fig. 1, where the (101) peak of the hexagonal phase is shown. This fact is clear evidence of the formation of a solid solution in the HfB<sub>2</sub>-ZrB<sub>2</sub> system. Moreover, the shift of XRD peaks shown in the onset of Fig. 1(a), which is attributed to different compositions in the solid solution, proves that the MSR process is able to control the stoichiometry of this solid solution by adjusting the starting Hf/Zr atomic ratio in the reactant mixture. On the other hand, diboride solid solutions were also obtained in samples 7 and 10

containing SiC as an additive. These are also possible to synthesize by MSR powdered ceramic matrix composites (CMCs) in an easy, reliable, and controlled way, where the main phase can be described as Hf<sub>1-x</sub>Zr<sub>x</sub>B<sub>2</sub>.

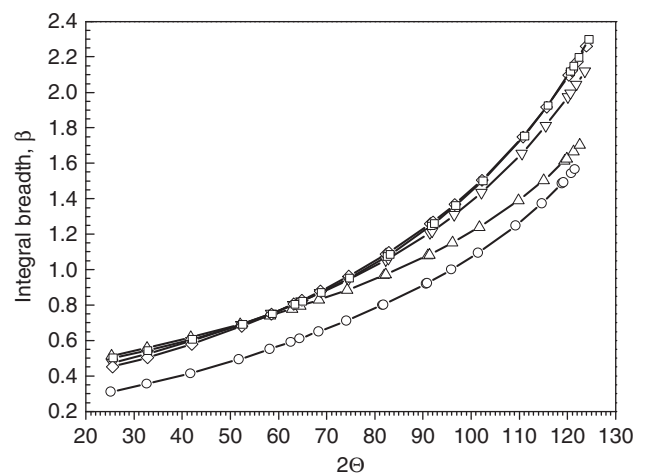
The lattice parameters of different hexagonal diboride phases obtained by MSR were calculated from the entire XRD patterns, and are shown in Fig. 3 and in Table III together with the *c/a* ratio and the cell volume. Lattice parameters (*a* and *c*) for samples 1, 6, and 9 (containing HfB<sub>2</sub>) agree with those of the JCPDS data file 38-1398 (HfB<sub>2</sub>), and those of samples 5, 8, and 11 (containing ZrB<sub>2</sub>) with lattice parameters of the JCPDS data file 34-0423 (ZrB<sub>2</sub>). On the other hand, *a* and *c* parameters for samples 2, 3, 4, 7, and 10 are between those of ZrB<sub>2</sub> and HfB<sub>2</sub>, confirming the formation of solid solutions in the ZrB<sub>2</sub>-HfB<sub>2</sub> system. The lattice parameters of diboride solid solutions show a nearly linear dependence on composition. The deviation observed in *a* and *c* parameters for samples 7 and 10 was the consequence of the formation of HfC, which results in a solid solution with a composition slightly richer in zirconium.

The broadening of the XRD peaks for samples 1–5 were compared (Fig. 4) in order to detect the solid solutions' fluctuations in the lattice spacing due to compositional heterogeneities. The existence of compositional heterogeneities would induce a nonhomogeneous broadening of the XRD peaks because the fluctuations in the lattice spacing depend on the crystallographic direction considered, being higher for those directions where the *d*-spacing corresponding to the end members are more divergent. However, Fig. 4 shows a similar tendency for the binary and ternary compounds suggesting that solid solutions are homogeneous from a stoichiometric point of view. The only difference observed was that ZrB<sub>2</sub> had narrower XRD peaks than HfB<sub>2</sub>, suggesting larger particle size. Broadening for solid solutions was between HfB<sub>2</sub> and ZrB<sub>2</sub>. On the other hand, the

**Table III.** Lattice Parameters (*a* and *c*), *c/a* Ratio, Cell Volumes (*V*), Crystallite Size (*D*), and Maximum Strain (*e*) of Hexagonal Diboride Phases Formed by the MSR Process. Space Group *P6/mmm* (191)

Sample	<i>a</i> = <i>b</i> (Å)	<i>c</i> (Å)	<i>V</i> (Å <sup>3</sup> )	<i>c/a</i>	<i>D</i> (nm)	<i>e</i> (× 10 <sup>-3</sup> )
1	3.1480(1)	3.4822(4)	29.884	1.106	20	3.92
2	3.1515(3)	3.4901(8)	30.019	1.107	17	2.86
3	3.1542(9)	3.4954(4)	30.116	1.108	21	3.83
4	3.1630(1)	3.5126(8)	30.433	1.111	24	4.23
5	3.1693(9)	3.5292(9)	30.699	1.114	37	3.23
6	3.1443(8)	3.4831(9)	29.822	1.108	15	2.67
7	3.1589(5)	3.5092(8)	30.325	1.111	21	3.94
8	3.1695(2)	3.5306(3)	30.715	1.114	36	2.21
9	3.1460(7)	3.4855(5)	29.874	1.108	14	3.67
10	3.1581(5)	3.5097(5)	30.314	1.111	17	3.03
11	3.1689(3)	3.5316(6)	30.712	1.114	35	3.12

MSR, mechanically induced self-sustaining reaction.

**Fig. 4.** Integral breadth of the X-ray powder diffraction peaks of products obtained after the mechanically induced self-sustaining reaction process for samples 1–5 in Table I. □, sample 1; △, sample 2; ▽, sample 3; ◇, sample 4; ○, sample 5.

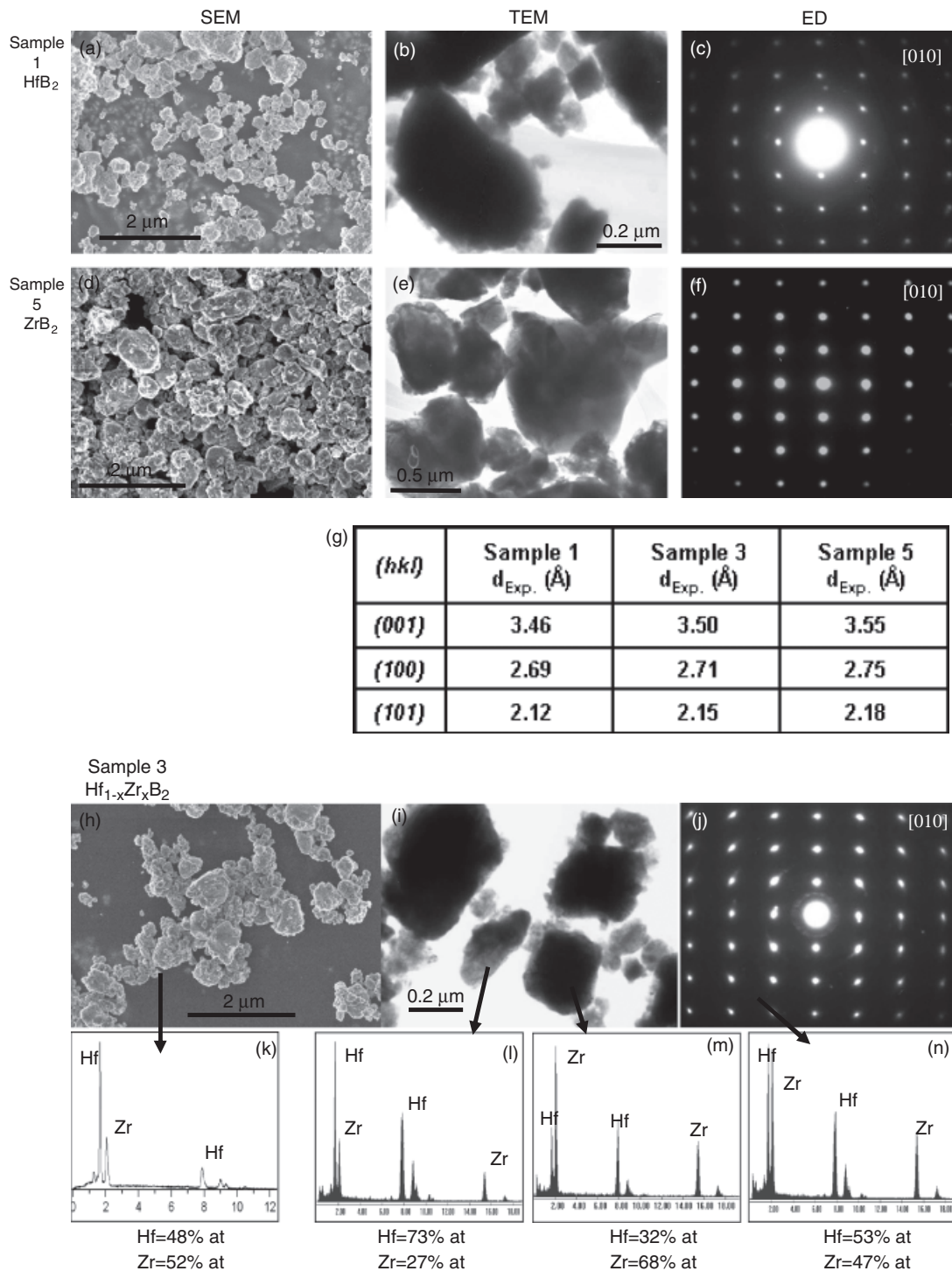


**Fig. 5.** Scanning electron microscopy (SEM), transmission electron microscopy, (TEM), electron diffraction (ED), and energy-dispersive X-ray (EDX) results for the diboride phases corresponding to (a–c) sample 1, (h–n) sample 3, and (d–f) sample 5. In the table (g), some  $d$ -spacing corresponding to the [010] zone axis of the three diboride phases are compared.

broadening of the XRD peaks suggested that diboride phases were obtained with a nanometric microstructure. The size of the coherently diffracting domain and the maximum strain are shown in Table III, where this tendency of smaller crystallite sizes for samples containing hafnium is observed.

The microstructural characterization of samples was performed using SEM and TEM techniques. The results for diboride samples are depicted in Fig. 5, where samples 1, 3, and 5 are compared (the ends and the middle term of the solid solution). SEM (Figs. 5(a), (d), and (h)) and TEM micrographs (Figs. 5(b), (e), and (i)) show that particle size increases with the zirconium content. The combination of TEM and ED techniques allowed us to determine the approximate size of

the diffracting domains using the size of the selected area aperture, and observe if the ED was rings or point patterns. It was also found that the dimensions of these domains were smaller for  $\text{HfB}_2$  (size range: 0.02–0.3  $\mu\text{m}$ ) than for  $\text{ZrB}_2$  (size range: 0.04–1  $\mu\text{m}$ ). The  $d$ -spacing corresponding to the [010] zone axis were measured for the three samples in the corresponding ED patterns (Figs. 5(c), (f), and (j)) and compared in the table (Fig. 5(g)). The  $d_{001}$ ,  $d_{100}$ , and  $d_{101}$  values for sample 3 are in between those corresponding to the  $\text{HfB}_2$  and  $\text{ZrB}_2$  samples, which confirm the formation of the  $\text{Hf}_{1-x}\text{Zr}_x\text{B}_2$  solid solution in fine agreement with the results from XRD.

EDX analysis was performed in both TEM and SEM microscopes and the spectra are shown in Figs. 5(k)–(n). The average

composition in sample 3 was 50/50 for Hf/Zr as confirmed by the EDX spectrum (Fig. 5(k)) obtained with the SEM microscope with a beam spot size of  $\sim 5 \mu\text{m}$ . However, the composition in each particle as determined by EDX in the TEM microscope showed that the Hf/Zr ratio was not strictly homogeneous. In some cases, higher compositions in Zr (Fig. 5(l)) or in Hf (Fig. 5(m)) were observed. Nevertheless, most of the EDX spectrum showed nearly 50% from each metal (Fig. 5(n)).

The results obtained for samples 2 and 4 were comparable with sample 3 in terms of mixed composition of Hf and Zr in each diboride particle, although the EDX spectra showed, as expected, that sample 2 was richer in Hf and sample 4 in Zr. However, the average diffracting domain in sample 2 was nearer to sample 1 ( $HfB_2$ ) and sample 4 was closer to sample 5 ( $ZrB_2$ ). This result seems to indicate that a higher quantity of Zr in the starting mixture submitted to high-energy ball milling implies larger crystalline diffraction domains in the final product, in agreement with XRD results. The values of the adiabatic temperature and formation enthalpy for  $ZrB_2$  and  $HfB_2$

are similar. However, if we consider the peak height of the pressure–time record as a direct measurement of the exothermic character of the MSR process, we noticed that this character was superior in those mixtures containing zirconium, which can induce a higher grain growth and explain the larger domain size observed in  $ZrB_2$ .

The TEM and SEM studies corresponding to the composite samples 6–11 are presented in Figs. 6(a)–(q), where representative SEM and TEM micrographs, ED patterns, and EDX spectra are shown. Different contrast can be clearly seen in SEM and TEM micrographs due to the presence of different phases in the composite material. For example, in TEM micrographs (Figs. 6(c), (i), (o), and (p)), the diboride phase appears with a darker contrast, and SiC with a lighter one (as confirmed by EDX). As in the previous samples, SEM micrographs showed larger particle sizes for the composite materials containing zirconium (Figs. 6(a), (g), and (m)). The results obtained for samples 6 ( $HfB_2+10 \text{ vol}\% \text{ SiC}$ ) and 9 ( $HfB_2+20 \text{ vol}\% \text{ SiC}$ ) were very similar in terms of microstructure and crystallinity. In

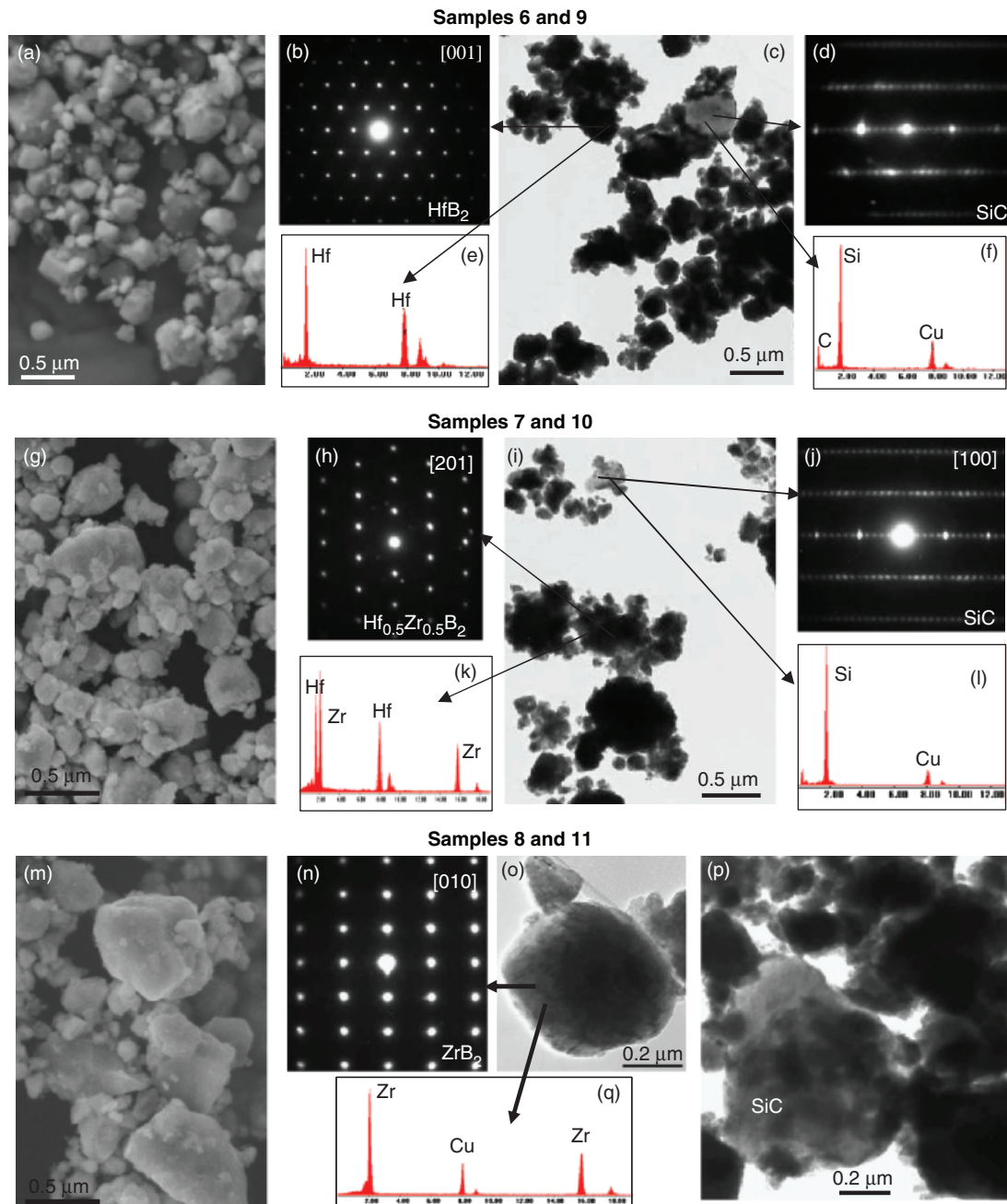


**Fig. 6.** Scanning electron microscopy, transmission electron microscopy, electron diffraction, and energy-dispersive X-ray results for the composite powders: (a–f) samples 6 and 9, (g–l) samples 7 and 10, and (m–q) samples 8 and 11.

the TEM micrograph, two crystallites were diffracted (Figs. 6(b) and (d)) and analyzed by EDX (Figs. 6(e) and (f)). One of them was assigned to the [001] zone axis of  $\text{HfB}_2$ , and the other one corresponded to the [100] zone axis of SiC (hexagonal system,  $P63mc$ , 186). The average diffracting domain of the diboride phase observed (by TEM and ED) was between 0.1 and 0.4  $\mu\text{m}$ . A polyhedral shape of particles was clearly observed in the SEM micrograph (Fig. 6(a)), and the average size was in the same range as observed in TEM (0.1–0.4  $\mu\text{m}$ ).

The composite samples 7 and 10 formed by the  $\text{Hf}_{1-x}\text{Zr}_x\text{B}_2$  solid solution phase plus 10 or 20 vol% of SiC, respectively, presented similar morphology, and representative micrographs, ED patterns, and EDX spectra are depicted in Figs. 6(g)–(l). Like in the previous composites, different crystallites corresponding to the diboride solid solution and SiC phases (marked with arrows) were analyzed using ED and EDX techniques. The ED pattern shown in Fig. 6(h) for the diboride phase was taken along the [201] zone axis and its corresponding EDX spectrum showed a similar composition in Hf and Zr (Fig. 6(k)).

Finally, the composite samples 8 and 11 formed by  $\text{ZrB}_2$  and 10 or 20 vol% of SiC, respectively, were also microcharacterized by the same techniques and representative results can be seen in Figs. 6(m)–(q). It was found that the diffracting domains of the diboride phase were larger than in the previous composite samples containing Hf. This fact is in agreement with the results for sample 5 from a microstructural point of view, confirming that larger particles are always associated with the  $\text{ZrB}_2$  formation.

#### IV. Conclusions

Hafnium and zirconium diborides and their solid solutions were obtained by milling elemental powder blends of hafnium, zirconium, and boron under inert atmosphere. An MSR was observed and full conversion was achieved for short milling times ( $\sim 30$  min). The stoichiometry of the solid solution was controlled by adjusting the Hf/Zr/B atomic ratio in the starting reactant mixture. The overall compositional range in  $\text{Hf}_{1-x}\text{Zr}_x\text{B}_2$  is available by means of this simple, direct, and time-efficient method.

$\text{HfB}_2$ -SiC,  $\text{ZrB}_2$ -SiC, and  $\text{Hf}_{1-x}\text{Zr}_x\text{B}_2$ -SiC composite materials were also obtained by adding the required amount of SiC to the elemental reactant mixture. Adding up to 20 vol% of SiC reduced the adiabatic temperature of the reactant mixture by 10%, and the formation of diboride phases by MSR was not inhibited. Longer milling times were necessary in order to ignite the reactant mixture as the amount of SiC was increased. HfC or ZrC was observed in the composite material as a direct consequence of the self-sustaining reaction, which induces the decomposition of SiC and the subsequent formation of carbides. The chemical, structural, and microstructural characterization of products confirmed the formation of  $\text{Hf}_{1-x}\text{Zr}_x\text{B}_2$  solid solutions with uniform chemical composition and submicrometric microstructure.

#### Acknowledgment

The authors wish to thank Ms. C. Gallardo for her assistance in the high-energy ball-milling experiments.

#### References

<sup>1</sup>R. Telle, L. S. Sigl, and K. Takagi, "Transition Metal Boride Ceramics"; pp. 803–945 in *Handbook of Ceramic Hard Materials*, Vol. 2, Edited by R. Riedel. Wiley-VCH, Weinheim, Germany, 2000.

<sup>2</sup>M. M. Opeka, I. G. Talmy, and J. A. Zaykoski, "Oxidation-Based Materials Selection for 2000°C+ Hypersonic Aerosurfaces: Theoretical Considerations and Historical Experience," *J. Mater. Sci.*, **39**, 5887–904 (2004).

<sup>3</sup>M. M. Opeka, I. G. Talmy, E. J. Wuchina, J. A. Zaykoski, and S. J. Causey, "Mechanical, Thermal, and Oxidation Properties of Refractory Hafnium and Zirconium Compounds," *J. Eur. Ceram. Soc.*, **19**, 2405–14 (1999).

<sup>4</sup>Sandia National Laboratories, "Ultra-High-Temperature Ceramics to Withstand 2000 Degrees Celsius," *ScienceDaily*, October 21, 2003. Available at <http://www.sciencedaily.com/releases/2003/10/031020055530.htm> (accessed January 2, 2008).

<sup>5</sup>S. R. Levine, E. J. Opila, M. C. Halbig, J. D. Kiser, M. Singh, and J. A. Salem, "Evaluation of Ultra-High Temperature Ceramics for Aero-propulsion Use," *J. Eur. Ceram. Soc.*, **22**, 2757–67 (2002).

<sup>6</sup>W. C. Tripp, H. H. Davis, and H. C. Graham, "Effect of SiC Addition on the Oxidation of  $\text{ZrB}_2$ ," *Am. Ceram. Soc. Bull.*, **52**, 612–6 (1973).

<sup>7</sup>F. Monteverde and A. Bellosi, "The Resistance to Oxidation of  $\text{HfB}_2$ -SiC Composite," *J. Eur. Ceram. Soc.*, **25**, 1025–31 (2005).

<sup>8</sup>W. G. Fahrenholtz, G. E. Hilmas, I. G. Talmy, and J. A. Zaykoski, "Refractory Diborides of Zirconium and Hafnium," *J. Am. Ceram. Soc.*, **90**, 1347–64 (2007).

<sup>9</sup>G. V. Samsonov, Y. M. Goryachev, and B. A. Kovenskaya, "Electronic Structure and Chemical Bonding in Transition Element Borides," *J. Less Common Metals*, **47**, 147–56 (1976).

<sup>10</sup>F. Monteverde, A. Bellosi, and L. Scatteia, "Processing and Properties of Ultra-High Temperature Ceramics for Space Applications," *Mater. Sci. Eng. A*, **485**, 415–21 (2008).

<sup>11</sup>M. Binnewies and E. Milke, *Thermochemical Data of Elements and Compounds*. Wiley-VCH, Weinheim, Germany, 1999.

<sup>12</sup>S. K. Mishra, S. Das, and L. C. Pathak, "Defect Structures in Zirconium Diboride Powder Prepared by Self-Propagating High-Temperature Synthesis," *Mater. Sci. Eng. A*, **364**, 249–55 (2004).

<sup>13</sup>N. Bertolino, M. Monagheddu, A. Tacca, P. Giuliani, C. Zanotti, F. Maglia, and U. Anselmi-Tamburini, "Self-propagating High-Temperature Synthesis of Functionally Graded Materials as Thermal Protection Systems for High-Temperature Applications," *J. Mater. Res.*, **18**, 448–55 (2003).

<sup>14</sup>J. M. Córdoba, M. J. Sayagués, M. D. Alcalá, and F. J. Gotor, "Monophasic  $\text{Ti}_y\text{Nb}_{1-y}\text{C}_x\text{N}_{1-x}$  Nanopowders Obtained at Room Temperature by MSR," *J. Mater. Chem.*, **17**, 650–3 (2007).

<sup>15</sup>J. M. Córdoba, M. A. Avilés, M. J. Sayagués, M. D. Alcalá, and F. J. Gotor, "Synthesis of Complex Carbonitride Powders  $\text{Ti}_y\text{M}_{1-y}\text{C}_x\text{N}_{1-x}$  (M: Zr, V, Ta, Hf) Via a Mechanically-Induced Self-Sustaining Reaction," *J. Alloys Comp.*, **482**, 349–55 (2009).

<sup>16</sup>J. M. Córdoba, M. J. Sayagués, M. D. Alcalá, and F. J. Gotor, "Monophasic Nanostructured Powders of Niobium, Tantalum, and Hafnium Carbonitrides Synthesized by a Mechanically Induced Self-Propagating Reaction," *J. Am. Ceram. Soc.*, **90**, 381–7 (2007).

<sup>17</sup>L. Takacs, "Self-Sustaining Reactions Induced by Ball Milling," *Prog. Mater. Sci.*, **47**, 355–414 (2002).

<sup>18</sup>L. Takacs, "Milling-Induced Combustion in Powder Mixtures Containing Titanium, Zirconium, or Hafnium," *J. Solid State Chem.*, **125**, 75–84 (1996).

<sup>19</sup>D. D. Radev and D. Klissurski, "Mechanochemical Synthesis and SHS of Diborides of Titanium and Zirconium," *J. Mater. Synth. Process.*, **9**, 131–6 (2001).

<sup>20</sup>P. Peshev and G. Bliznakov, "On the Boro-thermic Preparation of Titanium, Zirconium, and Hafnium Diborides," *J. Less-Common Metals*, **14**, 23–32 (1968).

<sup>21</sup>Z. Jiang and W. E. Rhine, "Preparation of Titanium Diboride from Titanium Alkoxide and Boron Powder," *Chem. Mater.*, **4**, 497–500 (1992).

<sup>22</sup>H. Maeda, T. Yoshikawa, K. Kusakabe, and S. Morooka, "Synthesis of Ultrafine  $\text{NbB}_2$  Powder by Rapid Carbo-thermal Reduction in a Vertical Tubular Reactor," *J. Alloys Comp.*, **215**, 127–34 (1994).

<sup>23</sup>Y. Xie, T. H. Sanders Jr., and R. F. Speyer, "Solution-Based Synthesis of Submicrometer  $\text{ZrB}_2$  and  $\text{ZrB}_2$ - $\text{TaB}_2$ ," *J. Am. Ceram. Soc.*, **91**, 1469–74 (2008).

<sup>24</sup>J. Inagaki, Y. Sakai, N. Uekawa, T. Kojima, and K. Kakegawa, "Synthesis and Evaluation of  $\text{Zr}_{0.5}\text{Ti}_{0.5}\text{B}_2$  Solid Solution," *Mater. Res. Bull.*, **42**, 1019–27 (2007).

<sup>25</sup>M. Moriyama, H. Aoki, and Y. Kobayashi, "Recent Developments of the Program Fullprof," *J. Ceram. Soc. Jpn.*, **106**, 1196–200 (1998).

<sup>26</sup>M. Shibuya, M. Kawata, M. Ohyanagi, and Z. A. Munir, "Titanium Diboride-Tungsten Diboride Solid Solution Formed by Induction-Field-Activated Combustion Synthesis," *J. Am. Ceram. Soc.*, **85**, 706–10 (2003).

<sup>27</sup>J. Rodriguez-Carvajal, "Recent Developments of the Program Fullprof," in *Commission on Powder Diffraction (IUCr), Newsletter*, **26**, 12–9 (2001).

<sup>28</sup>H. P. Klug and L. E. Alexander, *X-Ray Diffraction Procedures: For Polycrystalline and Amorphous Materials*, 2nd edition, John Wiley & Sons, New York, 1974.

<sup>29</sup>Z. A. Munir, "Synthesis of High-temperature Materials by Self-Propagating Combustion Methods," *Am. Ceram. Soc. Bull.*, **67**, 342–9 (1988).

<sup>30</sup>R. C. Weast ed., *Handbook of Chemistry and Physics*, 64th edition, CRC Press Inc., Boca Raton, FL, 1983.

<sup>31</sup>L. I. Berger, *Semiconductor Materials*. CRC Press, New York, 1997, p. 107. □